Research Square

Preprints are preliminary reports that have not undergone peer review.
They should not be considered conclusive, used to inform clinical practice,
or referenced by the media as validated information.

Induction of walnut callus and physiological and molecular differences among tissues with varying degrees of browning

Xinlin Huang
Zhejiang Sci-Tech University
Qinxiang Chang
Taiyuan University
Zongsuo Liang
Liangzs@ms.iswc.ac.cn

Zhejiang Sci-Tech University

Research Article

Keywords: Juglans regia, callus induction, tissue browning, tissue culture, TTC reduction, gene expression

Posted Date: November 6th, 2026

DOI: https://doi.org/10.21203/rs.3.rs-11383025/v1

License: This work is licensed under a Creative Commons Attribution 4.0 International License.
Read Full License

Additional Declarations: No competing interests reported.

Abstract

Immature cotyledons from ‘Xiangling’ walnut (*Juglans regia* L.) donor trees were used to screen callus induction conditions and characterize six browning grades (S1–S6). Single-factor experiments with three biological replicates per concentration identified 1 mg L^{-1} α-naphthaleneacetic acid, 0.5 mg L^{-1} 6-benzyladenine, and 200 mg L^{-1} ascorbic acid as the concentrations yielding the highest mean induction rates in their respective screens (87.8%, 85.6%, and 88.9%). At these concentrations, approximately 11% of induced calli exhibited more severe browning (S4–S6), while 62%–64% showed some browning (S2–S6). Morphological observations, histology, a 40 min 2,3,5-triphenyltetrazolium chloride (TTC) reduction assay, and reverse transcription quantitative polymerase chain reaction provided complementary assessments of tissue condition. Mean apparent TTC reduction activity decreased from 1409.4 ± 42.8 in S1 to 275.6 ± 13.1 μg TTC equivalents g^{-1} fresh weight h^{-1} in S5. The eight candidate embryogenesis-related genes reached their highest mean expression in S2–S4: *JrSERK1*and *JrBBM1* in S2; *JrBBM2* and *JrLEC2* in S3; and *JrLEC1*, *JrAGL15*, *JrFUS3*, and *JrWOX2* in S4. *JrLEC2* reached 9.86-fold relative to uncultured cotyledons. In S6, *JrSERK1*and *JrBBM1* expression was below control levels, whereas the other six genes remained elevated. Histology revealed variation in cell arrangement, staining, and tissue continuity. These findings identify favorable induction conditions and characterize browning-associated physiological and molecular variation, providing a basis for prioritizing S2–S4 for embryogenic competence assessment and subsequent regeneration studies.

Key Message

Single-factor screening identified favorable induction conditions, while integrated tissue assessment revealed distinct physiological and candidate-gene expression profiles across walnut callus browning grades.

1 Introduction

Persian walnut (*Juglans regia* L.) is economically important for nut and timber production, but its in vitro propagation is constrained by genotype-dependent responses and difficulties in culture establishment and regeneration (Vahdati et al. 2022). Recent advances in walnut genome editing further emphasize the need for responsive genotypes and reliable regeneration systems (Song et al. 2025). When cultures originate from immature seeds, the identity of the maternal cultivar must be distinguished from the genotype of each embryo. Here, cotyledon-derived callus was obtained from immature fruits collected from ‘Xiangling’ donor trees.

Walnut tissue culture protocols have been developed for several purposes. Genotype and basal medium influence the micropropagation of Persian walnut cultivars (Yegizbayeva et al. 2021), while other protocols support rooting and micrografting of Paradox rootstocks or short-term conservation through synthetic seed technology (Ribeiro et al. 2022; Sota et al. 2023). These studies demonstrate the value of

maintaining responsive tissues, but their outcomes cannot be directly extrapolated to cotyledon-derived callus or used to infer regenerative capacity from browning grade.

Immature walnut cotyledons can undergo somatic embryogenesis and plant regeneration (Tulecke and McGranahan 1985). Induction responses have also been characterized in immature cotyledons and embryos of ‘Xiangling’ (Cai et al. 2013), and subsequent work in apomictic walnut linked embryo induction to germination and plant recovery (Fang et al. 2022). These responses depend on basal nutrition, growth regulators, and the sequence of culture conditions (Phillips and Garda 2019). Callus formation must therefore be distinguished from the acquisition of embryogenic competence (Fehér 2019).

Browning is a major obstacle to maintaining responsive walnut cultures. Antioxidant treatments have been investigated in Persian walnut (Bhat et al. 2022). In *Juglans mandshurica*, browning during callus induction was associated with phenylalanine ammonia-lyase activity, polyphenols, and polyphenol oxidase (Liu et al. 2024a). Transcriptomic, metabolomic, and functional analyses of walnut stem explants also implicated phenolic oxidation and *JrPPO2* (Wang et al. 2025). These studies provide insight into browning mechanisms, but the relationship between visible browning, metabolic activity, and developmental gene expression in cotyledon-derived callus remains unclear.

Antioxidants, adsorbents, and adjustments to culture conditions are commonly used to control tissue browning, although their effectiveness depends on the explant and culture system (Amente and Chimdessa 2021; Permadi et al. 2024). Browning suppression and induction responses have also been examined in peony petal cultures (Cai et al. 2020). Genotype and environment influence phenolic metabolism and redox processes in woody plants (Liu et al. 2024b). Visible browning can inform assessments of tissue condition, but additional measurements are needed to connect it with biochemical mechanisms.

Developmental reprogramming involves hormonal responses and transcriptional networks (Ikeuchi et al. 2019). In *Arabidopsis*, BBM can activate the LEC1–ABI3–FUS3–LEC2 network, while auxin biosynthesis supports the maintenance and growth of BBM-induced embryos (Horstman et al. 2017a; Li et al. 2022). Related regulators participate in both zygotic and somatic embryogenesis (Salaün et al. 2021). Transcript abundance can therefore provide molecular evidence of tissue state, but it is insufficient on its own to establish embryogenic competence in walnut callus.

The cellular origin and regeneration pathway also require consideration. Organogenesis and somatic embryogenesis can follow distinct reprogramming trajectories, and callus formation does not indicate completion of either process (Ikeuchi et al. 2016; Ibáñez et al. 2020). Interpreting transcriptional evidence of somatic embryogenesis requires attention to tissue context, regulatory interactions, and developmental progression (Horstman et al. 2017b; Elhiti and Stasolla 2022).

We first evaluated the effects of NAA, 6-BA, and VC concentrations on callus induction and browning. We then compared apparent TTC activity and the expression of eight candidate embryogenesis-related

genes among six browning grades, alongside macroscopic and histological characterization. The study examined whether the least-browned callus also exhibited the highest apparent TTC activity and candidate transcript abundance. S1–S6 denote tissue grades at sampling, rather than medium treatments or successive developmental stages.

2 Materials and methods

2.1 Plant material and explant preparation

Immature fruits were collected from six 8-year-old ‘Xiangling’ walnut trees in the walnut industrial park of Kouqian Village, Yecun Town, Shangzhou District, Shangluo City, Shaanxi Province, China (110.0964° E, 33.7712° N; approximately 910 m above sea level). On 25 June 2026, approximately 65 days after peak female flowering, 36 fruits were harvested and transported under refrigeration to the laboratory within 18 h. Fruits from the six trees were pooled before processing.

Fruits were soaked in neutral detergent solution for 30 min with gentle scrubbing, rinsed under running water for 1 h, and drained. Under a laminar flow hood, they were immersed in 75% ethanol for 30 s, disinfected in sodium hypochlorite solution containing 1% available chlorine for 15 min, and rinsed five times with sterile distilled water. Immature embryos were excised aseptically, the seed coats were removed, and the cotyledons were cut into 2–4 mm pieces.

2.2 Culture media and subculture

All single-factor screens used DKW basal medium (Driver and Kuniyuki 1984) supplemented with 30 g L^{-1} sucrose and 7 g L^{-1} agar. The pH was adjusted to 5.8 before autoclaving at 121°C for 20 min. The NAA screen tested 0, 0.5, 1, 2, and 4 mg L^{-1} NAA with 6-BA fixed at 0.5 mg L^{-1} and no added VC. The 6-BA screen tested 0, 0.25, 0.5, 1, and 2 mg L^{-1} 6-BA with NAA fixed at 1 mg L^{-1} and no added VC. The VC screen tested 0, 100, 200, 400, and 600 mg L^{-1} VC with NAA and 6-BA fixed at 1 and 0.5 mg L^{-1}, respectively. The heat-labile VC stock solution was filter-sterilized and added after the medium had cooled to 50–55°C. Within each screen, all other medium components and culture conditions were held constant. Callus induction was conducted in darkness at 25 ± 2°C.

Vigorously growing callus was subcultured every 12 days for six consecutive passages. The maintenance medium consisted of DKW supplemented with 0.1 mg L^{-1} NAA, 1.0 mg L^{-1} 6-BA, 30 g L^{-1} sucrose, and 7 g L^{-1} agar (pH 5.8), with 100 mg L^{-1} VC and 1.0 g L^{-1} polyvinylpyrrolidone (PVP-30). Visibly necrotic tissue was removed at each subculture. Cultures were maintained in darkness at 25 ± 2°C.

Each concentration in the single-factor screens comprised three biological replicates of 30 explants each. The zero-concentration group served as the control for the factor being tested, with the specified background supplements retained. The three screens were analyzed separately. This design evaluated concentration effects within each fixed medium background but did not test interactions among factors.

At 12 days after inoculation, all callus-producing explants in each replicate were counted and classified as S1–S6. Callus induction was calculated as 100 × I/E, where E is the initial number of explants and I is the number that produced callus. Each callus-producing explant was counted as one induced callus unit, so I equaled the sum of the six grade counts. The proportion of induced calli showing any browning was calculated as $100 \times (n_2 + n_3 + n_4 + n_5 + n_6)/I$, where n_2–n_6 denote the counts in the corresponding grades. The proportion showing more severe browning was calculated as $100 \times (n_4 + n_5 + n_6)/I$ and included calli with > 30% browned surface area. Both browning measures were conditional on callus induction and excluded explants that did not produce callus. Grade counts are provided in Online Resource 1, Table S9. All supplementary tables and figures are included in Online Resource 1.

2.3 Browning grades and experimental units

Callus was classified into six grades according to color, texture, browned surface area, and growth status (Table 1). S1 described non-browned callus with vigorous growth; S6 described dark-brown to black, necrotic callus with > 80% browned surface area and no proliferative capacity. S2–S5 represented intermediate conditions. These operational criteria were used for visual assessment of tissue status.

Table 1
Operational grading criteria for walnut callus browning and growth status.

Grade	Browned area	Color and texture	Recorded growth and viability
S1	0%	Tender yellow or pale green; loose and plump; no visible browning.	Most vigorous growth.
S2	0 < B < 10%	Light yellow with a few localized brown spots.	Growth largely normal.
S3	10% ≤ B ≤ 30%	Localized browning; most tissue remains active.	Capable of continued proliferation.
S4	30% < B ≤ 50%	Extensive brown regions.	Activity markedly reduced.
S5	50% < B ≤ 80%	Predominantly browned tissue with small fresh portions.	Only a small proportion remains fresh and viable.
S6	B > 80%	Dark brown to black; necrotic tissue.	No proliferative capacity.

B is the visually assessed percentage of browned surface area within an individual callus piece. Growth and viability descriptions are the recorded criteria for assigning tissue status, not percentages derived from the TTC assay. S1–S6 denote grades rather than medium treatments. The six-grade thresholds are operational criteria for this study.

Three biological replicates per callus grade were used for the TTC and RT-qPCR analyses. Fresh, uncultured cotyledons served as the RT-qPCR control and retained the sample label WT. Histological specimens were selected by macroscopic appearance and were not assigned to S1–S6. Multiple microscopic fields from a specimen were used for morphological description and were not treated as independent biological replicates.

2.4 TTC reduction assay

Apparent TTC reduction activity was measured using a modified plant root activity assay kit (Boxbio, Beijing, China; AKPL029M) adapted for walnut callus. Residual medium was removed from tissue surfaces, samples were rinsed three times with distilled water, and surface moisture was blotted dry. Each biological replicate included a reaction sample and a paired control. Their fresh weights were recorded separately because reaction and control masses differed (Table S1).

Each sample received 1000 μL of Working Solution I. Paired controls received 250 μL of Reagent IV before incubation to inhibit TTC reduction and measure background absorbance. Samples were incubated in darkness at 37°C for 40 min, after which 250 μL of Reagent IV was added to the reaction tubes to stop the reaction.

Tissue was removed from the reaction solution, blotted, and ground in 1 mL of ethyl acetate to extract triphenylformazan. The homogenate and ethyl acetate rinsings were combined, adjusted to 2 mL, and centrifuged at 15,000 × g for 10 min at 4°C. A 200 μL aliquot of supernatant was transferred to an ethyl acetate-resistant, non-polystyrene 96-well plate, and absorbance was measured at 485 nm.

Nominal TTC-equivalent standards of 5, 10, 20, 30, 40, and 50 μg mL^{-1} were prepared by reduction and extraction of the kit standard. Two measurement series were corrected using their respective ethyl acetate blanks, and the means at each concentration were used for linear calibration. A third series measured after 1 h at room temperature was retained separately (Table S2). Sample absorbance was calculated as $\Delta A = A_{485,\text{reaction}} - A_{485,\text{control}}$, without adjustment for unequal reaction and control masses.

The calibration equation was $\Delta A = 0.0202589x + 0.00256164$, where x is the TTC-equivalent concentration in μg mL^{-1}. Apparent activity was calculated as $(x \times V)/(W \times T)$, where V = 2 mL, W is the individual reaction fresh weight in grams, and T = 40/60 h. Under these conditions, activity = 3x/W, expressed as μg TTC equivalents g^{-1} fresh weight h^{-1}. This quantity describes TTC reduction under the assay conditions; it is not the percentage of viable cells. S6 was not assigned a quantitative activity because its background-corrected signal was not consistently positive. Grade-level summaries are reported in Table 2.

Table 2
Apparent TTC reduction across walnut callus browning grades after a 40 min incubation.

Grade	n	ΔA mean ± SD	Activity mean ± SD
S1	3	0.8997 ± 0.0379	1409.4 ± 42.8 a
S2	3	0.5417 ± 0.0150	907.3 ± 43.0 b
S3	3	0.4757 ± 0.0278	798.6 ± 77.7 bc
S4	3	0.3803 ± 0.0117	532.8 ± 3.0 c
S5	3	0.2180 ± 0.0219	275.6 ± 13.1 d
S6	3	-0.0083 ± 0.0190	Not quantified

Activity units: μg TTC equivalents g^{-1} FW h^{-1}. Values use individual reaction fresh weights and unadjusted paired control absorbance. Letters following activity means indicate Holm-adjusted pairwise Welch comparisons: groups sharing a letter did not differ at adjusted $P < 0.05$. S6 was not included in quantitative activity comparisons.

2.5 Histological examination

Histological specimens comprised milky-white friable callus, pale-yellow callus, brownish-yellow compact callus, slightly browned callus, severely browned callus, and uncultured immature embryos. Samples were fixed in FAA fixative (Servicebio, China) at room temperature for 24 h. Dehydration, clearing, paraffin embedding, sectioning at 4 μm, staining, and digital scanning were performed by Wuhan Servicebio Technology Co., Ltd.

After deparaffinization and rehydration, sections were stained with 0.5% toluidine blue (G1032, Servicebio) for 2–5 min and briefly rinsed with tap water. Differentiation with 0.1% acetic acid was performed when required by the staining results. Sections were dried at 60°C, cleared in xylene for 10 min, and mounted in neutral resin. Images were acquired using a 20× objective at a pixel size of 0.273810 μm. Representative overview fields and enlarged views were selected and provided with scale bars. Image processing was limited to cropping, proportional resizing, and annotation.

2.6 RNA extraction and RT-qPCR

Expression of eight candidate embryogenesis-related genes (*JrSERK1*, *JrBBM1*, *JrBBM2*, *JrLEC1*, *JrLEC2*, *JrAGL15*, *JrFUS3*, and *JrWOX2*) was examined in S1–S6 callus and fresh, uncultured cotyledons (WT). Control cotyledons were obtained from immature fruits at the same developmental stage as the experimental explants. Each group comprised three independent biological replicates. Total RNA was extracted using the RNAprep Pure Plant kit (Tiangen, China; DP441). RNA concentration, purity, and integrity were assessed by NanoDrop spectrophotometry and 1.0% agarose gel electrophoresis. Acceptance criteria were an A_{260}/A_{280} ratio of 1.8–2.1 and intact 28S and 18S rRNA bands. Residual genomic DNA was removed by on-column DNase I digestion. First-strand cDNA was synthesized from 1000 ng of total RNA using the HiScript III qPCR reverse transcription kit with gDNA wiper (Vazyme, China; R323) and diluted tenfold before RT-qPCR.

RT-qPCR was performed using a real-time PCR instrument with ChamQ SYBR qPCR Master Mix (Vazyme, Q712-02). Each 10 μL reaction contained 5.0 μL of 2× master mix, 0.4 μL each of forward and reverse primers (10 μM stocks; 0.4 μM final concentration each), 1.0 μL of cDNA, and 3.2 μL of nuclease-free water. The amplification program comprised 95°C for 30 s, followed by 40 cycles of 95°C for 10 s and 60°C for 30 s, with fluorescence acquisition at 60°C. Melting-curve analysis comprised 95°C for 15 s and 60°C for 1 min, followed by a ramp to 95°C at 0.5°C s^{-1} with continuous fluorescence acquisition.

Gene accession numbers, forward and reverse primer sequences (5'–3'), and expected amplicon lengths are listed in Table S5. *JrTIP41* was the sole reference gene used for normalization. Primer information and Ct measurements for *JrEF1A* and *JrACT* are also reported, but these genes were not used to calculate relative expression. Table S6 presents the three biological-replicate Ct values for each reference-gene candidate within each group, together with the mean and sample SD. CK and WT denote the same uncultured control. All supplementary tables and figures are provided in Online Resource 1.

Three independent biological samples per group were analyzed, with separate RNA extraction and reverse transcription. Each biological sample was assayed in three technical wells per gene, and mean Cq values were used for normalization. For each target gene, ΔCt was calculated by subtracting the matched *JrTIP41* Ct from the target-gene Ct. The mean WT ΔCt was used as the calibrator, giving ΔΔCt = sample ΔCt − mean WT ΔCt. Relative expression was calculated using the $2^{-\Delta\Delta Ct}$ method (Livak and Schmittgen 2001), which assumes similar target and reference amplification efficiencies close to 100%. Biological replicates were the units of statistical analysis; technical replicates and pooled controls across batches were not counted as independent observations. Expression results are reported as mean ± SD of three biological replicates. Individual ΔCt values and expression summaries are provided in Table S7, and comparisons between each callus grade and WT are reported in Table S8.

2.7 Statistical analysis

TTC activity and relative gene expression are summarized as mean ± SD for three biological replicates per group. Exploratory TTC comparisons among S1–S5 used Welch's ANOVA, followed by two-sided pairwise Welch tests with Holm adjustment across the ten group comparisons. S6 was excluded from quantitative activity comparisons. For each gene, comparisons against WT used two-sided Welch tests on biological-replicate ΔCt values, with Holm adjustment across the six comparisons within that gene. Adjusted $P < 0.05$ was used as the significance threshold. Expression summaries were calculated on the $2^{-\Delta\Delta Ct}$ scale, while hypothesis tests used ΔCt. Macroscopic and histological observations were descriptive. For the supplementary reanalysis, two-sided 95% confidence intervals for each TTC grade mean were calculated using the Student t distribution with two degrees of freedom. These are pointwise intervals conditional on the calibration and assay procedure, not simultaneous confidence intervals and not estimates of total measurement uncertainty. Ratios to the S1 mean are descriptive summaries of the same data, not independent outcomes (Table S3). Full pairwise results are provided in Table S4. For the single-factor screens, replicate percentages were calculated from integer counts before rounding and summarized as mean ± sample SD (n = 3). Exploratory Welch one-way ANOVA compared five

concentrations separately for each factor and each of three endpoints. Holm adjustment covered all nine omnibus tests (Table S10). Numerator degrees of freedom were four; denominator degrees of freedom were estimated separately for each test. No post hoc concentration comparisons or interaction tests were performed. The small number of biological replicates limits assessment of distributional assumptions.

For heatmap visualization, $\log_2$ relative expression was calculated as mean WT ΔCt minus sample ΔCt, and the three biological-replicate values were averaged within each group. Heatmap values therefore represent − ΔΔCt, equivalent to the $\log_2$ of geometric mean relative expression, rather than the $\log_2$ of the arithmetic mean fold changes shown in the gene-specific plots. A common color scale centered on zero was used without row-wise standardization or hierarchical clustering. Groups were retained in the order WT, S1–S6. The heatmap was generated using Matplotlib and provides a descriptive summary; statistical inference remained based on the ΔCt comparisons described above.

ChatGPT (OpenAI) assisted with manuscript organization, language editing, and preparation of analysis and visualization scripts. Numerical analyses used recorded experimental measurements; no experimental observations were generated using AI. The authors retain responsibility for the interpretation and final content of the manuscript.

3 Results

3.1 Single-factor effects on callus induction and browning

The three single-factor screens comprised 15 factor–concentration combinations, each with three biological replicates (Online Resource 1, Table S9). Table 3 reports induction as a percentage of initial explants and the two browning measures as percentages of induced callus units. Exploratory Welch ANOVA indicated concentration effects for all nine factor–endpoint combinations after Holm adjustment (maximum adjusted P = 0.000589; Online Resource 1, Table S10). These omnibus tests assess overall concentration effects within each screen.

Table 3
Callus induction and browning-grade proportions in the single-factor screens.

Factor	mg L^{-1}	n	Induction (%)	S2–S6 / I (%)	S4–S6 / I (%)
NAA	0	3	58.9 ± 1.9	83.0 ± 0.6	45.3 ± 1.5
NAA	0.5	3	83.3 ± 3.3	64.0 ± 1.4	16.0 ± 0.6
NAA	1	3	87.8 ± 1.9	62.0 ± 0.8	11.4 ± 0.2
NAA	2	3	70.0 ± 3.3	77.8 ± 2.0	34.9 ± 1.5
NAA	4	3	51.1 ± 1.9	86.9 ± 0.5	50.0 ± 3.3
6-BA	0	3	54.4 ± 1.9	81.6 ± 0.6	44.9 ± 1.9
6-BA	0.25	3	81.1 ± 1.9	67.1 ± 0.8	16.4 ± 0.4
6-BA	0.5	3	85.6 ± 1.9	63.6 ± 1.9	11.7 ± 0.3
6-BA	1	3	68.9 ± 1.9	75.8 ± 0.7	33.9 ± 1.0
6-BA	2	3	47.8 ± 1.9	86.0 ± 0.5	51.1 ± 1.9
VC	0	3	74.4 ± 1.9	77.6 ± 0.6	46.2 ± 1.4
VC	100	3	85.6 ± 1.9	68.8 ± 0.7	19.5 ± 0.4
VC	200	3	88.9 ± 1.9	62.5 ± 0.8	11.3 ± 0.2
VC	400	3	87.8 ± 1.9	65.8 ± 0.7	15.2 ± 0.3
VC	600	3	71.1 ± 1.9	71.9 ± 0.7	25.0 ± 2.0

Values are mean ± sample SD of three biological-replicate percentages calculated from integer counts before rounding. Each replicate contained 30 initial explants. I denotes induced callus units. Induction = 100 × I/30; S2–S6/I includes all browned grades, and S4–S6/I includes more severe browning (> 30% browned surface area). Numerical extrema are descriptive; no pairwise significance letters are assigned. Fixed medium backgrounds are specified in Section 2.2.

In the NAA screening experiment, the 1 mg L^{-1} concentration yielded the highest mean induction rate (87.8 ± 1.9%) and the lowest mean proportions of overall browning (grades S2–S6; 62.0 ± 0.8%) and more severe browning (grades S4–S6; 11.4 ± 0.2%). Similarly, in the 6-BA screening experiment, the 0.5 mg L^{-1} concentration performed best, achieving an induction rate of 85.6 ± 1.9%, with browning proportions of 63.6 ± 1.9% (grades S2–S6) and 11.7 ± 0.3% (grades S4–S6). With fixed basal concentrations of 1 mg L^{-1} NAA and 0.5 mg L^{-1} 6-BA, the addition of 200 mg L^{-1} VC resulted in the highest mean induction rate (88.9 ± 1.9%) and the lowest proportions of browning for grades S2–S6 (62.5 ± 0.8%) and S4–S6 (11.3 ± 0.2%).

At the concentrations with the most favorable means in each screen, induction exceeded 85%, while approximately 11% of induced calli were classified as S4–S6. Overall browning occurred in 62%–64% of induced calli and was predominantly represented by grades S2–S3. These results identify useful starting

conditions for medium development. Concentration rankings describe mean responses; pairwise concentration differences and interactions among factors were not tested.

3.2 Macroscopic variation in callus appearance

Walnut callus tissues exhibited diverse macroscopic characteristics regarding color, shape, and surface texture. Light-colored callus developed on the surfaces and edges of green explants, forming circular protrusions with lobed margins (Fig. 1A–C). Other samples displayed yellow-green or amber central regions surrounded by milky-white to pale yellow callus, with localized granular surface features (Fig. 1D–F).

Callus masses varied in shape—ranging from circular to irregular or elongated—and exhibited surface textures that were smooth, granular, or lobed (Fig. 2A–D). Browning varied in extent, ranging from localized patches to extensive dark brown discoloration (Fig. 2E, F). Light-colored callus coexisted with yellow-to-amber and distinctly browned tissues within the same Petri dish, demonstrating heterogeneity in tissue appearance within a single culture vessel (Fig. 3).

Further observations documented various callus morphologies and pigmentation patterns (Figs. S1 and S2). Additionally, an abnormal culture covered with abundant white, flocculent material was separately recorded (Fig. S2K). Collectively, these observations identified distinct macroscopic characteristics for describing walnut callus and provided a morphological basis for subsequent analyses of physiological and molecular properties.

3.3 Browning grades and growth status

The grading criteria distinguished pale-yellow or pale-green, friable and plump, non-browned callus (S1) from increasingly browned tissue (S2–S5) and extensively browned, necrotic tissue without recorded proliferation (S6; Table 1). Intermediate grades described sparse brown spots with largely normal growth (S2), retained active tissue capable of proliferation (S3), reduced activity (S4), and only small portions of fresh tissue (S5). These descriptions defined the categories; their frequencies in the induction screens are reported in Table 3.

3.4 Apparent TTC reduction activity

The blank-corrected calibration data were closely described by the linear equation $\Delta A = 0.0202589x + 0.00256164$ ($R^2 = 0.998867$; Online Resource 1, Fig. S3 and Table S2). Corrected absorbance values for S1–S5 ranged from 0.193 to 0.934 and lay within the measured calibration range.

Apparent TTC activity differed among S1–S5 (Welch ANOVA, $P = 1.12 \times 10^{-5}$; Table 2; Fig. 4). S1 showed the highest mean activity (1409.4 ± 42.8 μg TTC equivalents g^{-1} FW h^{-1}), exceeding all other quantified grades in Holm-adjusted pairwise comparisons. S5 showed the lowest mean activity (275.6 ± 13.1 μg TTC equivalents g^{-1} FW h^{-1}) and was lower than S1–S4. Mean activities in S2, S3, S4, and S5 were 64.4%, 56.7%, 37.8%, and 19.6% of the S1 mean, respectively. The difference between the S1 and S5 means

corresponded to an 80.4% decrease. S2–S3 and S3–S4 were not significantly different after adjustment. Grade-level summaries and full pairwise results are provided in Online Resource 1, Tables S3 and S4.

For S6, background-corrected absorbance values were 0.010, − 0.007, and − 0.028, with a mean ± SD of − 0.0083 ± 0.0190. Because the corrected signal was not consistently positive, S6 was reported as absorbance rather than assigned a quantitative TTC activity. These observations describe the signal under the assay conditions; they do not establish a formal detection limit or a cell-survival percentage.

3.5 Histological characteristics

Sections of uncultured young walnut embryo explants clearly revealed their original tissue structure: the tissue was continuous and intact, composed primarily of polygonal cells that varied in size and exhibited distinct outlines, pale cytoplasmic staining, and a translucent appearance (Fig. 5K, L). These results established a baseline reference for the cytological observation and comparative analysis of the callus tissues in this study.

The cultured callus specimens showed distinct structural characteristics (Fig. 5). Milky-white friable callus contained cells of variable size with lightly stained interiors (Fig. 5A, B). Pale-yellow callus combined small, densely stained cells with larger cells and showed local discontinuities (Fig. 5C, D). Brownish-yellow compact callus retained a relatively continuous structure with localized darker staining (Fig. 5E, F). Slightly browned callus showed irregular cell outlines and conspicuous intercellular spaces (Fig. 5G, H). Severely browned callus exhibited more fragmented tissue organization, although recognizable cell outlines remained in some regions (Fig. 5I, J).

Together, these specimens illustrate variation in cell arrangement, staining, and tissue continuity across the selected morphological categories. Histology adds structural information to the callus assessment; the categories were selected separately from the S1–S6 samples used for physiological and molecular comparisons.

3.6 Candidate gene expression profiles

The eight candidate embryogenesis-related genes exhibited distinct expression profiles across the sampled browning grades (Fig. 6). Relative to uncultured cotyledons (WT), *JrSERK1* expression was significantly higher in S1–S4, did not differ significantly in S5, and was significantly lower in S6. *JrBBM1* expression was significantly higher in S1–S5 and lower in S6. Both genes reached their highest mean expression in S2.

The remaining six genes (*JrBBM2*, *JrLEC2*, *JrLEC1*, *JrAGL15*, *JrFUS3*, and *JrWOX2*) were significantly more highly expressed than WT across all six callus grades. *JrBBM2* and *JrLEC2* reached their highest mean expression in S3, whereas *JrLEC1*, *JrAGL15*, *JrFUS3*, and *JrWOX2* reached their highest mean expression in S4. The heatmap summarizes these contrasting profiles on a common $\log_2$ scale (Fig. 7). Mean expression maxima were concentrated in S2–S4, while S6 combined lower-than-WT expression of *JrSERK1* and *JrBBM1* with higher-than-WT expression of the other six genes. These patterns distinguish

the sampled tissue states; S1–S6 represent browning grades rather than successive developmental time points. The reported significance tests compare each grade with WT, whereas the locations of expression maxima are descriptive.

The Ct values of the three reference-gene candidates, *JrEF1A*, *JrTIP41*, and *JrACT*, showed limited variation across WT and S1–S6 in the recorded measurements (Online Resource 1, Table S6). *JrTIP41* was the sole reference used for normalization. The replicate ΔCt values and full grade–WT comparisons are provided in Online Resource 1, Tables S7 and S8, respectively.

4 Discussion

4.1 Browning grades as a framework for tissue assessment

The highest mean apparent TTC activity occurred in S1, whereas the eight candidate embryogenesis-related genes reached their highest mean expression in S2, S3, or S4. This difference identifies complementary features of the sampled tissues: TTC reduction describes reductive activity under the assay conditions, while transcript abundance describes the selected gene-expression profiles. The combined observations prioritize intermediate grades for further evaluation of embryogenic competence. Because the grades were sampled cross-sectionally, these distributions do not establish a developmental sequence or an optimal induction time.

The S1–S6 scheme provides non-overlapping thresholds for assigning individual callus units to visual grades. It distinguishes the proportion of callus units affected by browning from the browned surface area within a unit, a distinction relevant to interpreting population-level induction assays (Duan et al. 2022). Reporting both S2–S6 and S4–S6 proportions further separates any visible browning from more severe browning. The criteria combine tissue color and texture with recorded growth status, providing an operational basis for selecting callus for further assessment.

The decline in mean apparent TTC activity across S1–S5 provides a physiological context for the visual grades. Phenolic metabolism and oxidase activity have been implicated in walnut explant browning (Liu et al. 2024a; Wang et al. 2025), and transcriptomic and metabolomic analyses have examined browning-associated changes in *Camellia hainanica* callus (Wu et al. 2024). Measuring phenolic content, oxidase activity, and oxidative damage in grade-matched walnut samples would test how these processes relate to the patterns reported here.

The single-factor screens identified favorable concentrations within defined medium backgrounds. In particular, the VC screen directly evaluated 200 mg L^{-1} VC on a background of 1 mg L^{-1} NAA and 0.5 mg L^{-1} 6-BA, yielding a mean induction rate of 88.9% and an S4–S6 proportion of 11.3%. This tested formulation provides a practical starting point for further culture development. Factorial experiments

would establish whether interactions among the components improve performance beyond the conditions evaluated here.

Light provides another potential axis for culture development. Its effects on plant regeneration involve hormonal responses and tissue development (Han et al. 2025), while transient light-quality treatments have been associated with browning and metabolic changes in tea tissue culture (Ding et al. 2025). The present dark-culture conditions provide a defined background for testing light treatments. Applying the same induction and browning measures would allow future comparisons without assuming that responses observed in other species transfer directly to walnut.

4.2 Interpretation and limitations of TTC reduction

TTC reduction adds a measurable physiological dimension to visual grading. Positive corrected signals in S1–S5 supported calculation of apparent reduction activity, and the grade means declined with increasing browning severity. S6 was retained in the report as corrected absorbance because it lacked a consistently positive signal. This distinction allows the measurements to be interpreted without equating near-zero corrected absorbance with a quantified absence of viable cells.

The activity calculation used each reaction sample's fresh weight and paired tissue-control absorbance. Reaction and control masses nevertheless differed, and no mass correction was applied to the background signal. In addition, the recorded calibration does not establish comparability across assay batches. These features constrain interpretation of the absolute activity values and may contribute to between-sample variation. Matching tissue masses and including contemporaneous standards would strengthen quantitative comparisons.

All activity estimates use a 40 min incubation. Under this fixed condition, the assay differentiated several grades, including S1 from S2–S5 and S5 from S1–S4. The nonsignificant S2–S3 and S3–S4 comparisons indicate that not every adjacent visual grade was resolved statistically. Additional biological replication and calibration of the assay against an independent viability measure would help define its discriminating ability across the full grading range.

4.3 Developmental identity and gene expression

Histology adds structural information to the macroscopic assessment of walnut callus. The milky-white friable specimen contained many cells with large, lightly stained interiors; a pale color and friable appearance therefore did not, by themselves, identify a population of embryogenic cells. The other specimens showed differences in cell arrangement, staining, and tissue continuity. Such differences are descriptive and cannot be equated with differences in division rate, cell viability, or developmental competence without additional measurements.

Callus is a heterogeneous tissue whose molecular state can include developmental competence without completed organ or embryo formation. Comparative analysis has identified a shared pre-meristematic molecular signature across plant calli (Fehér 2023), and transcriptome studies of two Eucalyptus

species have described distinct gene-expression programs during callus development (Zhang et al. 2022). These observations support pairing morphology with molecular measurements, while cautioning against assigning identity from a small marker panel alone.

TTC and histology address different aspects of tissue condition. The lack of a consistently positive TTC signal in S6 concerns reduction under the assay conditions, whereas recognizable outlines in a fixed, severely browned section concern preserved structure. Neither observation alone establishes the viability of every cell. The histological categories were not specimen-matched to the TTC grades, so no quantitative correspondence was inferred. Future sampling of adjacent portions of the same callus piece would allow stronger comparisons between structural condition and metabolic activity.

The uncultured embryo provides a tissue-of-origin comparison, not evidence that new embryos arose in culture. Rounded surfaces, locally dense staining, and expression of developmental regulators are insufficient individually to establish somatic embryogenesis (Fehér 2019). In established walnut regeneration studies, the evidence extends to embryo development and plant recovery (Tulecke and McGranahan 1985; Fang et al. 2022). The current observations should therefore be positioned as callus characterization, with embryogenic competence remaining a separate experimental question.

The expression profiles suggest that candidate developmental transcripts respond differently across the sampled tissue states. JrSERK1 and JrBBM1 peaked numerically in S2, JrBBM2 and JrLEC2 in S3, and JrLEC1, JrAGL15, JrFUS3, and JrWOX2 in S4. These are descriptive maxima, because the reported tests compared grades with WT rather than directly comparing all grades. Functional work in Arabidopsis links BBM to embryogenic regulatory networks and auxin-dependent embryo maintenance (Horstman et al. 2017a; Li et al. 2022), but BBM also participates in early seed and endosperm development (Chen et al. 2022). Thus, higher abundance of a candidate transcript relative to uncultured cotyledons cannot be equated with higher regeneration capacity in walnut callus.

The heatmap complements the gene-specific plots by displaying the distribution of candidate transcript abundance across all sampled grades on the same scale (Fig. 7). The concentration of expression maxima in S2–S4, alongside the highest apparent TTC activity in S1, illustrates that candidate transcript abundance and tissue reduction activity describe different aspects of callus condition. This integrated view supports prioritizing intermediate grades for tests of embryogenic competence, without assigning temporal or causal relationships to the cross-sectional expression patterns.

The gene panel includes regulators with different functions and regulatory inputs. Studies of AGL15 have linked embryogenic responses to auxin and gibberellin regulation (Zheng et al. 2016), while subsequent work places AGL15 within a broader developmental network (Joshi et al. 2022). A recent review likewise emphasizes both shared and distinct functions of transcription factors in zygotic and somatic embryogenesis (Yuan et al. 2024). The expression maxima of *JrAGL15*, *JrLEC1*, *JrFUS3*, and *JrWOX2* in S4 therefore warrant further investigation but do not establish that S4 callus is embryogenic.

Hormonal responses depend on timing and developmental context. Wound-induced callus formation involves dynamic hormone and transcriptional changes (Ikeuchi et al. 2017), and auxin–cytokinin interactions contribute to shoot-forming competence (Raspor et al. 2021). Structure–activity analysis of 2,4-D has linked auxinic activity to somatic embryo induction in Arabidopsis (Karami et al. 2023). Relating the culture conditions identified here to subsequent developmental responses would help connect medium composition with walnut regeneration.

Epigenetic regulation offers an additional hypothesis for variation in callus competence. PRC2 restricts hormone-induced embryogenesis in Arabidopsis vegetative tissue (Mozgová et al. 2017), while MET1-mediated DNA methylation is linked to cytokinin-induced cell-cycle regulation during shoot regeneration (Liu et al. 2018). Chromatin and DNA methylation analyses would extend the present expression-based characterization and test their contribution to walnut callus responses.

In the S6 samples, transcript levels of *JrSERK1* and *JrBBM1* were lower than in the uncultured cotyledon control (WT), whereas the levels of the remaining six transcripts remained high. This pattern necessitates careful consideration of the source and state of the RNA samples, particularly given that S6 is characterized as tissue exhibiting severe browning and necrosis, devoid of proliferative activity. Factors such as tissue composition, residual RNA, or normalization effects could be potential underlying causes. Furthermore, the interpretation of results depends on RNA quality, reference gene stability, primer specificity, and amplification efficiency, as emphasized by current qPCR reporting guidelines (Bustin et al. 2025).

Normalization merits particular attention. A walnut study found that suitable reference genes differed among organs, developmental stages, and cultivars (Zhou et al. 2018); it does not validate TIP41 across the browning grades examined here. The original MIQE recommendations and their 2025 revision both emphasize transparent assay reporting (Bustin et al. 2009, 2025). The reference-gene Ct measurements show a narrow observed range across groups (Table S6), but this alone does not establish normalization validity. The biological-replicate ΔCt records reproduce the expression summaries and comparisons with WT (Tables S7 and S8).

5 Conclusions

Within the tested concentration ranges, 1 mg L^{-1} NAA, 0.5 mg L^{-1} 6-BA, and 200 mg L^{-1} VC produced the most favorable mean induction and browning outcomes in their respective single-factor screens. At these concentrations, induction exceeded 85% and approximately 11% of induced calli were classified as S4–S6. Mean apparent TTC activity decreased across S1–S5, whereas candidate embryogenesis-related transcripts reached their highest mean abundance in S2–S4. The heatmap summarized these contrasting gene-expression profiles, and histology provided complementary descriptions of tissue organization. Together, the findings identify useful culture conditions and an integrated approach to walnut callus assessment. They prioritize intermediate browning grades for tests of embryogenic competence and provide a basis for subsequent somatic embryogenesis and regeneration studies.

Abbreviations

6-BA
6-benzyladenine
ANOVA
analysis of variance
Ct
threshold cycle
DKW
Driver and Kuniyuki medium
FW
fresh weight
NAA
α-naphthaleneacetic acid
RT-qPCR
reverse transcription quantitative polymerase chain reaction
SD
standard deviation
TTC
2,3,5-triphenyltetrazolium chloride
VC
ascorbic acid
WT
uncultured cotyledon control

Declarations

Competing interests

The authors declare that they have no competing interests.

Funding

This work was supported by Fundamental Research Program of Shanxi Province (Grant No. 202303021222227).

Author Contribution

X.H. performed the experiments, processed the data, and drafted the manuscript. Q.C. revised the manuscript and provided funding support. Z.L. provided experimental guidance and contributed to the

study concept.

Acknowledgements

The authors gratefully acknowledge the financial support from the Fundamental Research Program of Shanxi Province (Grant No. 202303021222227).

Data Availability

The data supporting the findings of this study are provided in the article and its supplementary information (Online Resource 1). These include TTC absorbance and fresh-weight measurements, calibration data, reference-gene Ct values, target-gene ΔCt values, and replicate-level callus induction and browning-grade counts.

References

1. Amente G, Chimdessa E (2021) Control of browning in plant tissue culture: A review. J Sci Agric 5:67–71. https://doi.org/10.25081/jsa.2021.v5.7266
2. Bhat SN, Khalil A, Nazir N, Mir MA, Khan I, Mubashir SS, Dar MS, Wani SH, Hossain MA (2022) In Vitro Prevention of Browning in Persian Walnut (Juglans regia L.) cv. Sulaiman. Int J Plant Biology 13:330–342. https://doi.org/10.3390/ijpb13030027
3. Bustin SA, Benes V, Garson JA, Hellemans J, Huggett J, Kubista M, Mueller R, Nolan T, Pfaffl MW, Shipley GL, Vandesompele J, Wittwer CT (2009) The MIQE Guidelines: Minimum Information for Publication of Quantitative Real-Time PCR Experiments. Clin Chem 55:611–622. https://doi.org/10.1373/clinchem.2008.112797
4. Bustin SA, Ruijter JM, van den Hoff MJB, Kubista M, Pfaffl MW, Shipley GL, Tran N, Rödiger S, Untergasser A, Mueller R, Nolan T, Milavec M, Burns MJ, Huggett JF, Vandesompele J, Wittwer CT (2025) MIQE 2.0: Revision of the Minimum Information for Publication of Quantitative Real-Time PCR Experiments Guidelines. Clin Chem 71:634–651. https://doi.org/10.1093/clinchem/hvaf043
5. Cai XD, Wang GY, Cao WJ (2013) In vitro Induction and Proliferation of Callus from Immature Cotyledons and Embryos of Juglans regia cv. 'Xiangling'. Notulae Botanicae Horti Agrobotanici Cluj-Napoca 41:378–384. https://doi.org/10.15835/nbha4129134
6. Cai X, Wei H, Liu C, Ren X, Thi LT, Jeong BR (2020) Synergistic Effect of NaCl Pretreatment and PVP on Browning Suppression and Callus Induction from Petal Explants of Paeonia Lactiflora Pall. ‘Festival Maxima’ Plants 9:346. https://doi.org/10.3390/plants9030346
7. Chen B, Maas L, Figueiredo D, Zhong Y, Reis R, Li M, Horstman A, Riksen T, Weemen M, Liu H, Siemons C, Chen S, Angenent GC, Boutilier K (2022) BABY BOOM regulates early embryo and endosperm development. Proceedings of the National Academy of Sciences 119:e2201761119. https://doi.org/10.1073/pnas.2201761119

8. Ding Y, Huang H, Zhao Y (2025) Metabolomics Reveals the Mechanism of Browning Inhibition by Transient Light Quality in Tea Plant Tissue Culture. Plants 14:3539. https://doi.org/10.3390/plants14223539
9. Driver JA, Kuniyuki AH (1984) In vitro propagation of Paradox walnut rootstock. HortScience 19:507–509. https://doi.org/10.21273/HORTSCI.19.4.507
10. Duan S, Xin R, Guan S, Li X, Fei R, Cheng W, Pan Q, Sun X (2022) Optimization of callus induction and proliferation of Paeonia lactiflora Pall. and Agrobacterium-mediated genetic transformation. Front Plant Sci 13:996690. https://doi.org/10.3389/fpls.2022.996690
11. Elhiti M, Stasolla C (2022) Transduction of Signals during Somatic Embryogenesis. Plants 11:178. https://doi.org/10.3390/plants11020178
12. Fang H, Dong Y, Zhou R, Wang Q, Duan Q, Wang C, Bao Y, Xu S, Lang X, Gai S, Chen R, Yang KQ (2022) Optimization of the induction, germination, and plant regeneration system for somatic embryos in apomictic walnut (Juglans regia L). Plant Cell Tissue Organ Cult (PCTOC) 150:289–297. https://doi.org/10.1007/s11240-022-02266-9
13. Fehér A (2019) Callus, Dedifferentiation, Totipotency, Somatic Embryogenesis: What These Terms Mean in the Era of Molecular Plant Biology? Front Plant Sci 10:536. https://doi.org/10.3389/fpls.2019.00536
14. Fehér A (2023) A Common Molecular Signature Indicates the Pre-Meristematic State of Plant Calli. Int J Mol Sci 24:13122. https://doi.org/10.3390/ijms241713122
15. Han J, Li Y, Zhao Y, Sun Y, Li Y, Peng Z (2025) How does light regulate plant regeneration? Front Plant Sci 15:1474431. https://doi.org/10.3389/fpls.2024.1474431
16. Horstman A, Li M, Heidmann I, Weemen M, Chen B, Muino JM, Angenent GC, Boutilier K (2017a) The BABY BOOM Transcription Factor Activates the LEC1-ABI3-FUS3-LEC2 Network to Induce Somatic Embryogenesis. Plant Physiol 175:848–857. https://doi.org/10.1104/pp.17.00232
17. Horstman A, Bemer M, Boutilier K (2017b) A transcriptional view on somatic embryogenesis. Regeneration 4:201–216. https://doi.org/10.1002/reg2.91
18. Ibáñez S, Carneros E, Testillano PS, Pérez-Pérez JM (2020) Advances in Plant Regeneration: Shake, Rattle and Roll. Plants 9:897. https://doi.org/10.3390/plants9070897
19. Ikeuchi M, Ogawa Y, Iwase A, Sugimoto K (2016) Plant regeneration: cellular origins and molecular mechanisms. Development 143:1442–1451. https://doi.org/10.1242/dev.134668
20. Ikeuchi M, Iwase A, Rymen B, Lambolez A, Kojima M, Takebayashi Y, Heyman J, Watanabe S, Seo M, De Veylder L, Sakakibara H, Sugimoto K (2017) Wounding Triggers Callus Formation via Dynamic Hormonal and Transcriptional Changes. Plant Physiol 175:1158–1174. https://doi.org/10.1104/pp.17.01035
21. Ikeuchi M, Favero DS, Sakamoto Y, Iwase A, Coleman D, Rymen B, Sugimoto K (2019) Molecular Mechanisms of Plant Regeneration. Annu Rev Plant Biol 70:377–406. https://doi.org/10.1146/annurev-arplant-050718-100434

22. Joshi S, Paul P, Hartman JM, Perry SE (2022) AGL15 Promotion of Somatic Embryogenesis: Role and Molecular Mechanism. Front Plant Sci 13:861556. https://doi.org/10.3389/fpls.2022.861556
23. Karami O, de Jong H, Somovilla VJ, Villanueva Acosta B, Sugiarta AB, Ham M, Khadem A, Wennekes T, Offringa R (2023) Structure–activity relationship of 2, 4-D correlates auxinic activity with the induction of somatic embryogenesis in Arabidopsis thaliana. Plant J 116:1355–1369. https://doi.org/10.1111/tpj.16430
24. Li M, Wrobel-Marek J, Heidmann I, Horstman A, Chen B, Reis R, Angenent GC, Boutilier K (2022) Auxin biosynthesis maintains embryo identity and growth during BABY BOOM-induced somatic embryogenesis. Plant Physiol 188:1095–1110. https://doi.org/10.1093/plphys/kiab558
25. Liu H, Zhang H, Dong YX, Hao YJ, Zhang XS (2018) DNA METHYLTRANSFERASE1-mediated shoot regeneration is regulated by cytokinin-induced cell cycle in Arabidopsis. New Phytol 217:219–232. https://doi.org/10.1111/nph.14814
26. Liu C, Li A, Fan X, Qin B, Zhang L (2024a) Explant browning during callus induction of Juglans mandshurica might be caused by the cooperation of PAL, polyphenol and PPO. South Afr J Bot 174:937–945. https://doi.org/10.1016/j.sajb.2024.09.072
27. Liu C, Fan H, Zhang J, Wu J, Zhou M, Cao F, Tao G, Zhou X (2024b) Combating browning: mechanisms and management strategies in in vitro culture of economic woody plants. Forestry Res 4:e032. https://doi.org/10.48130/forres-0024-0026
28. Livak KJ, Schmittgen TD (2001) Analysis of Relative Gene Expression Data Using Real-Time Quantitative PCR and the $2^{-\Delta\Delta CT}$ Method. Methods 25:402–408. https://doi.org/10.1006/meth.2001.1262
29. Mozgová I, Muñoz-Viana R, Hennig L (2017) PRC2 Represses Hormone-Induced Somatic Embryogenesis in Vegetative Tissue of Arabidopsis thaliana. PLoS Genet 13:e1006562. https://doi.org/10.1371/journal.pgen.1006562
30. Permadi N, Akbari SI, Prismantoro D, Indriyani NN, Nurzaman M, Alhasnawi AN, Doni F, Julaeha E (2024) Traditional and next-generation methods for browning control in plant tissue culture: Current insights and future directions. Curr Plant Biology 38:100339. https://doi.org/10.1016/j.cpb.2024.100339
31. Phillips GC, Garda M (2019) Plant tissue culture media and practices: an overview. In Vitro Cellular & Developmental Biology - Plant 55:242–257. https://doi.org/10.1007/s11627-019-09983-5
32. Raspor M, Motyka V, Kaleri AR, Ninković S, Tubić L, Cingel A, Ćosić T (2021) Integrating the Roles for Cytokinin and Auxin in De Novo Shoot Organogenesis: From Hormone Uptake to Signaling Outputs. Int J Mol Sci 22:8554. https://doi.org/10.3390/ijms22168554
33. Ribeiro H, Ribeiro A, Pires R, Cruz J, Cardoso H, Barroso JM, Peixe A (2022) Ex Vitro Rooting and Simultaneous Micrografting of the Walnut Hybrid Rootstock 'Paradox' (Juglans hindsi × Juglans regia) cl. 'Vlach' Agron 12:595. https://doi.org/10.3390/agronomy12030595
34. Salaün C, Lepiniec L, Dubreucq B (2021) Genetic and Molecular Control of Somatic Embryogenesis. Plants 10:1467. https://doi.org/10.3390/plants10071467

35. Song L, Zhang P, Gao R, Li B, Zheng Z, Song X, Pei D (2025) Walnut genome editing: an optimized CRISPR/Cas9 platform with superior genotypes and endogenous promoters. Hortic Res 12:uhaf187. https://doi.org/10.1093/hr/uhaf187
36. Sota V, Benelli C, Myrselaj M, Kongjika E, Gruda NS (2023) Short-Term Conservation of Juglans regia L. via Synthetic Seed Technology. Horticulturae 9:559. https://doi.org/10.3390/horticulturae9050559
37. Tulecke W, McGranahan G (1985) Somatic embryogenesis and plant regeneration from cotyledons of walnut, Juglans regia L. Plant Sci 40:57–63. https://doi.org/10.1016/0168-9452(85)90163-3
38. Vahdati K, Sadeghi-Majd R, Sestras AF, Licea-Moreno RJ, Peixe A, Sestras RE (2022) Clonal Propagation of Walnuts (Juglans spp.): A Review on Evolution from Traditional Techniques to Application of Biotechnology. Plants 11:3040. https://doi.org/10.3390/plants11223040
39. Wang H, Chen Z, An X, Wang H, Zhao S (2025) Comprehensive transcriptome and metabolomic analyses reveal the browning mechanism of walnut explants. Ind Crops Prod 225:120447. https://doi.org/10.1016/j.indcrop.2024.120447
40. Wu K, Liu Y, Xu Y, Yu Z, Cao Q, Gong H, Yang Y, Ye J, Jia X (2024) Unveiling the Molecular Mechanisms of Browning in Camellia hainanica Callus through Transcriptomic and Metabolomic Analysis. Int J Mol Sci 25:11021. https://doi.org/10.3390/ijms252011021
41. Yegizbayeva TK, García-García S, Yausheva TV, Kairova M, Apushev AK, Oleichenko SN, Licea-Moreno RJ (2021) Unraveling Factors Affecting Micropropagation of Four Persian Walnut Varieties. Agronomy 11:1417. https://doi.org/10.3390/agronomy11071417
42. Yuan HY, Kagale S, Ferrie AMR (2024) Multifaceted roles of transcription factors during plant embryogenesis. Front Plant Sci 14:1322728. https://doi.org/10.3389/fpls.2023.1322728
43. Zhang Y, Li J, Li C, Chen S, Tang Q, Xiao Y, Zhong L, Chen Y, Chen B (2022) Gene expression programs during callus development in tissue culture of two Eucalyptus species. BMC Plant Biol 22:1. https://doi.org/10.1186/s12870-021-03391-x
44. Zheng Q, Zheng Y, Ji H, Burnie W, Perry SE (2016) Gene Regulation by the AGL15 Transcription Factor Reveals Hormone Interactions in Somatic Embryogenesis. Plant Physiol 172:2374–2387. https://doi.org/10.1104/pp.16.00564
45. Zhou L, Niu J, Quan S (2018) Identification of appropriate reference genes for RT-qPCR analysis in Juglans regia L. PLoS ONE 13:e0209424. https://doi.org/10.1371/journal.pone.0209424

Figures

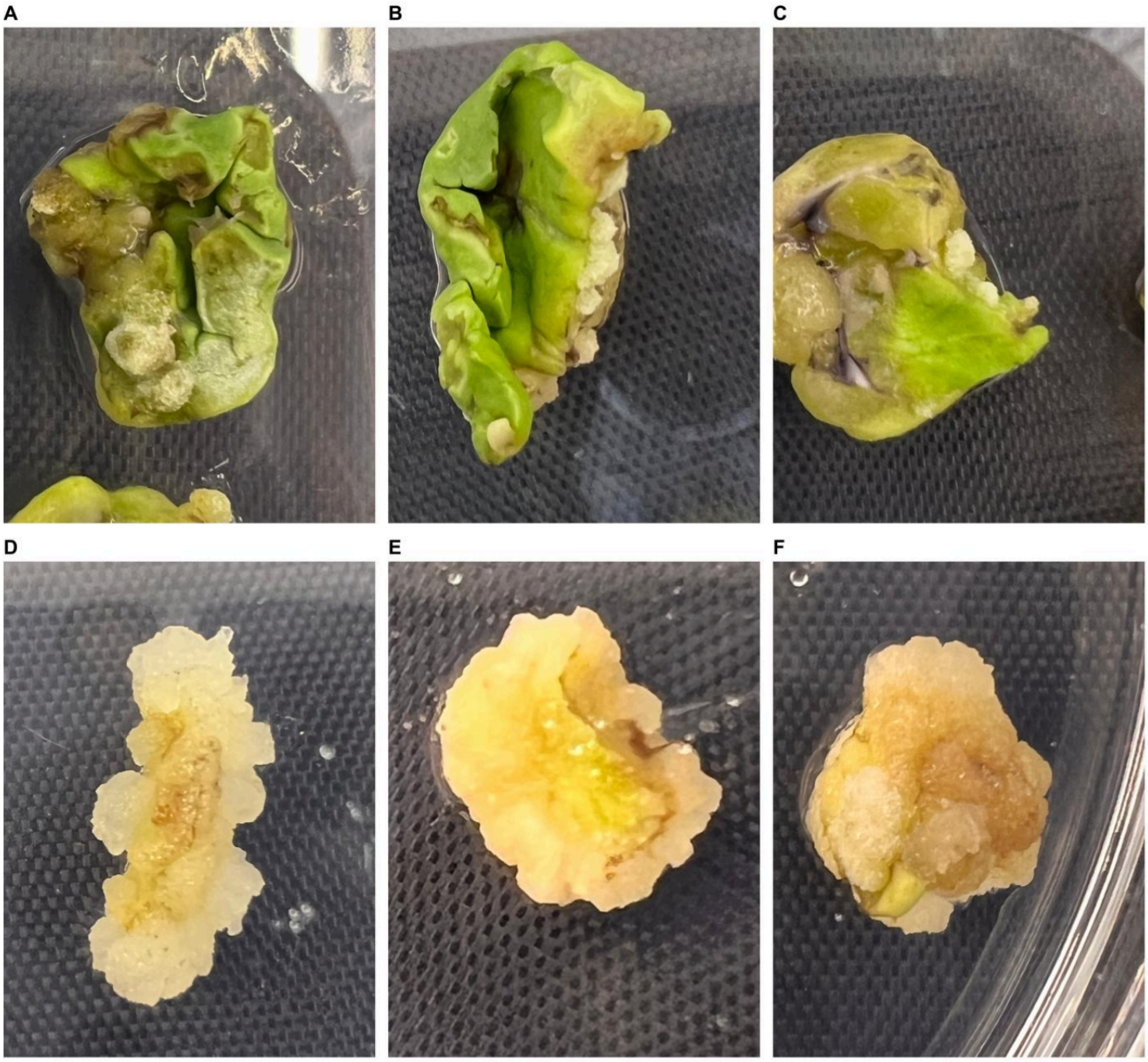


Figure 1

Explant-associated walnut callus. Panels A–F show pale rounded, lobed, or granular outgrowths associated with green or discolored explant tissue. Images describe tissue appearance; panels are not treated as a time series

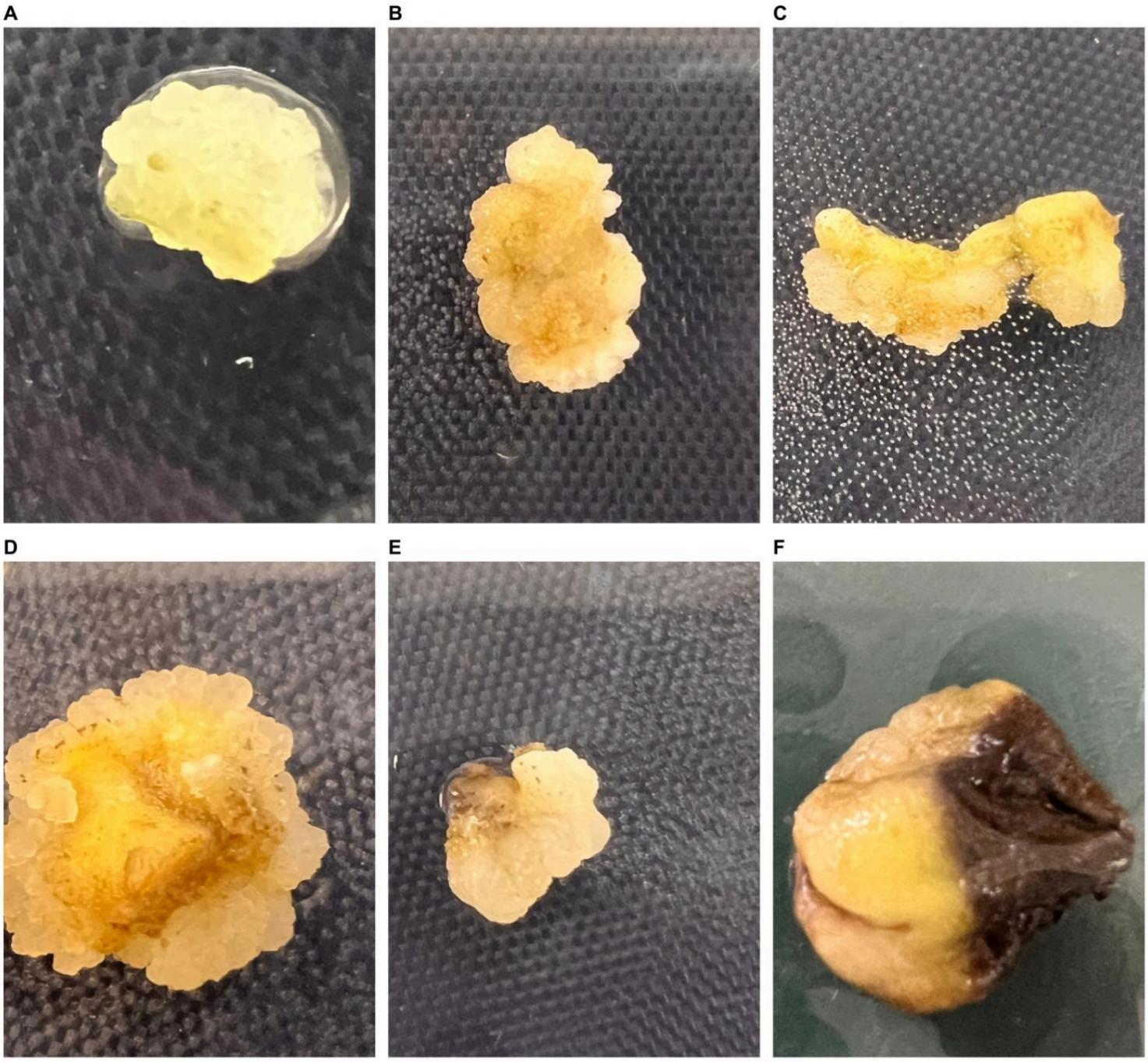


Figure 2

Variation in callus morphology and browning. A, pale rounded callus; B, irregular lobed tissue; C, elongated granular tissue; D, peripheral rounded outgrowths around an amber region; E, localized browning; F, extensively browned explant tissue

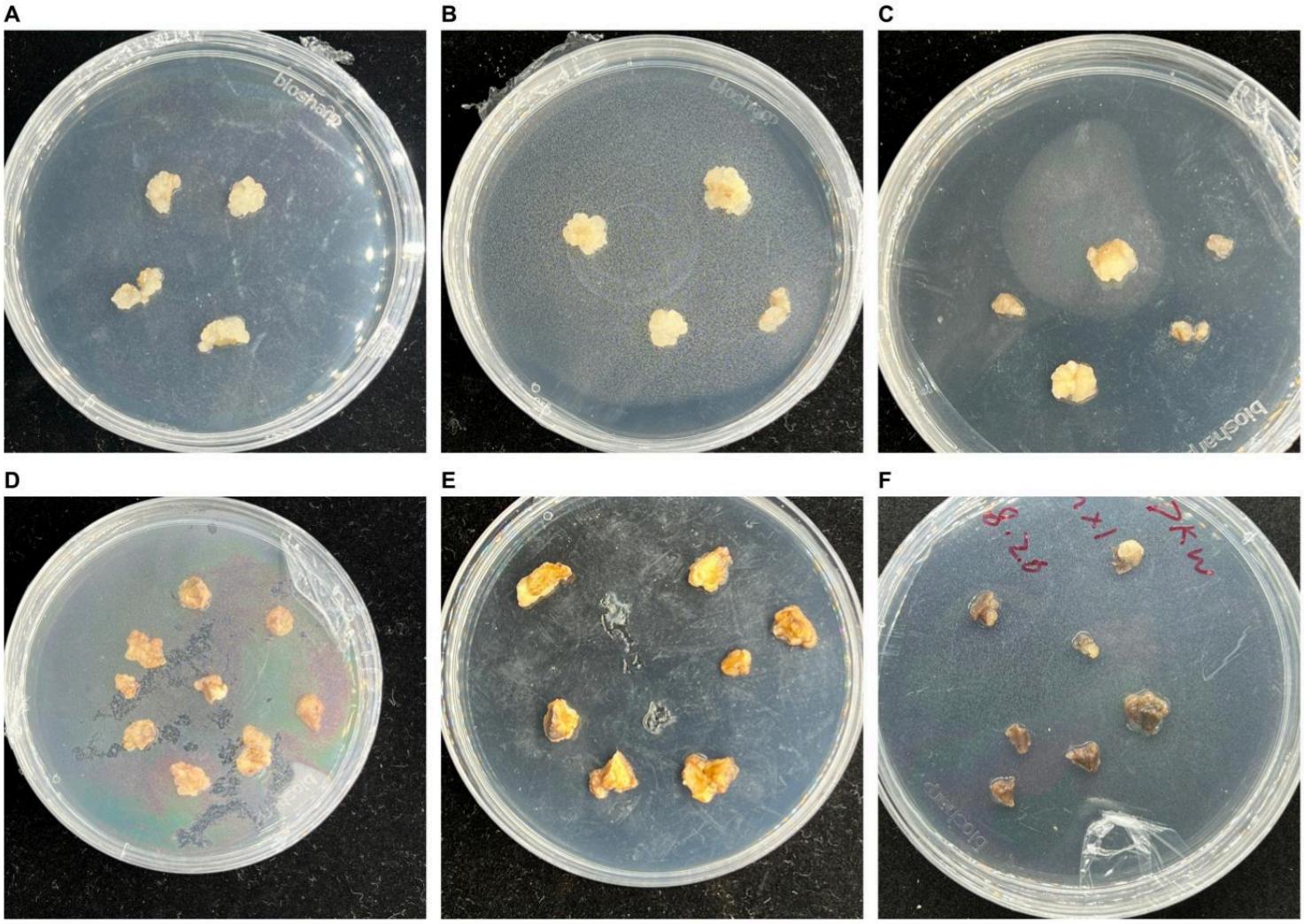


Figure 3

Dish-level appearance of walnut cultures. A–C, discrete cream to pale yellow tissues; D, yellow to amber tissues; E, yellow-orange tissues with localized browning; F, visibly browned tissues. The images are descriptive views and are not assigned to S grades without verified sample records

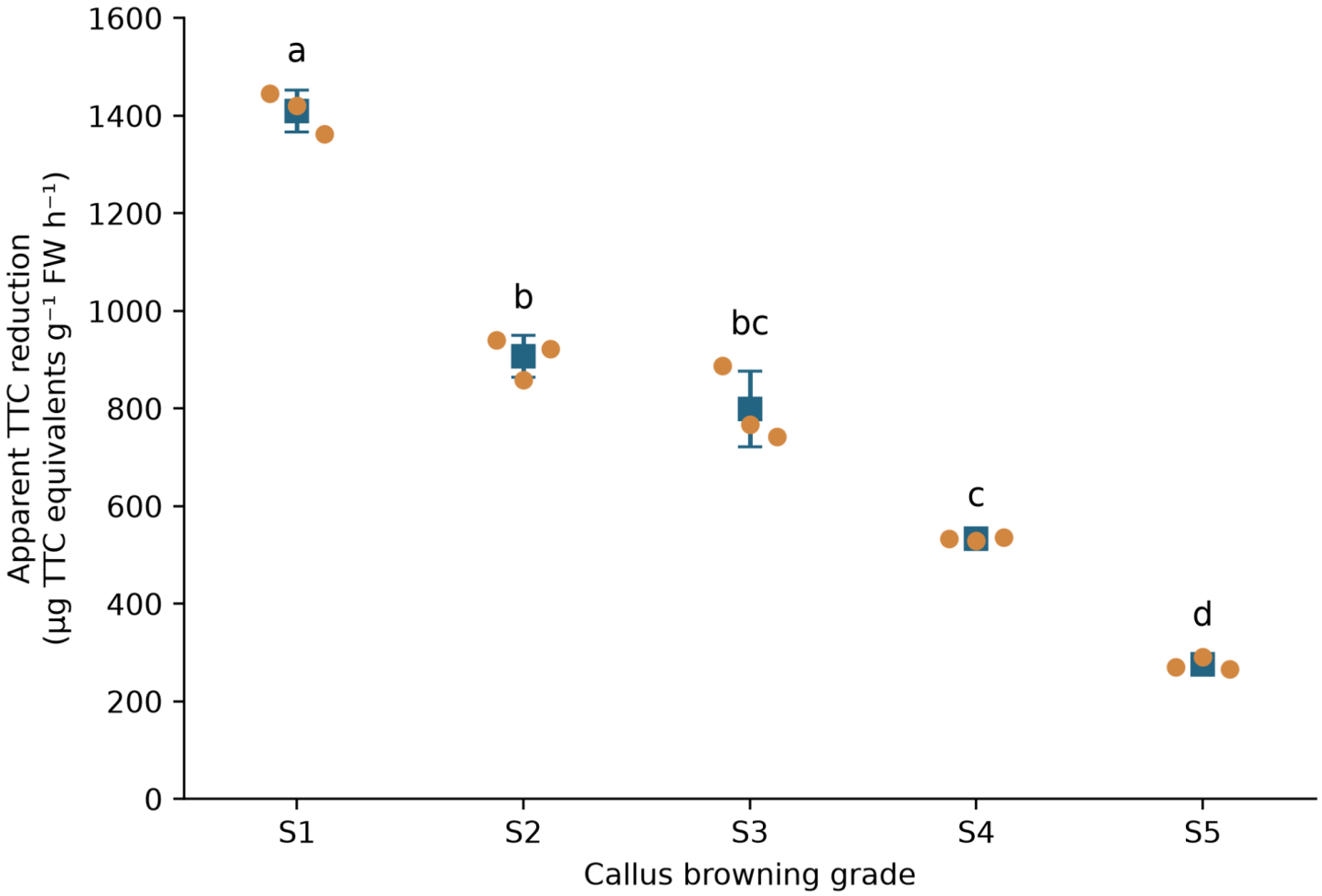


Figure 4

Apparent TTC reduction in walnut callus grades S1–S5. Orange points represent independent biological samples; blue squares and error bars indicate mean ± SD (n = 3). Values use a 40 min incubation, 2 mL extract volume, and individual reaction fresh weights. Different lowercase letters indicate significant pairwise differences after Holm adjustment; groups sharing a letter did not differ at adjusted $P < 0.05$. S6 is reported separately as corrected absorbance. Reaction and control masses differed (Online Resource 1, Table S1). Welch ANOVA indicated an overall difference among S1–S5 ($P = 1.12 \times 10^{-5}$)

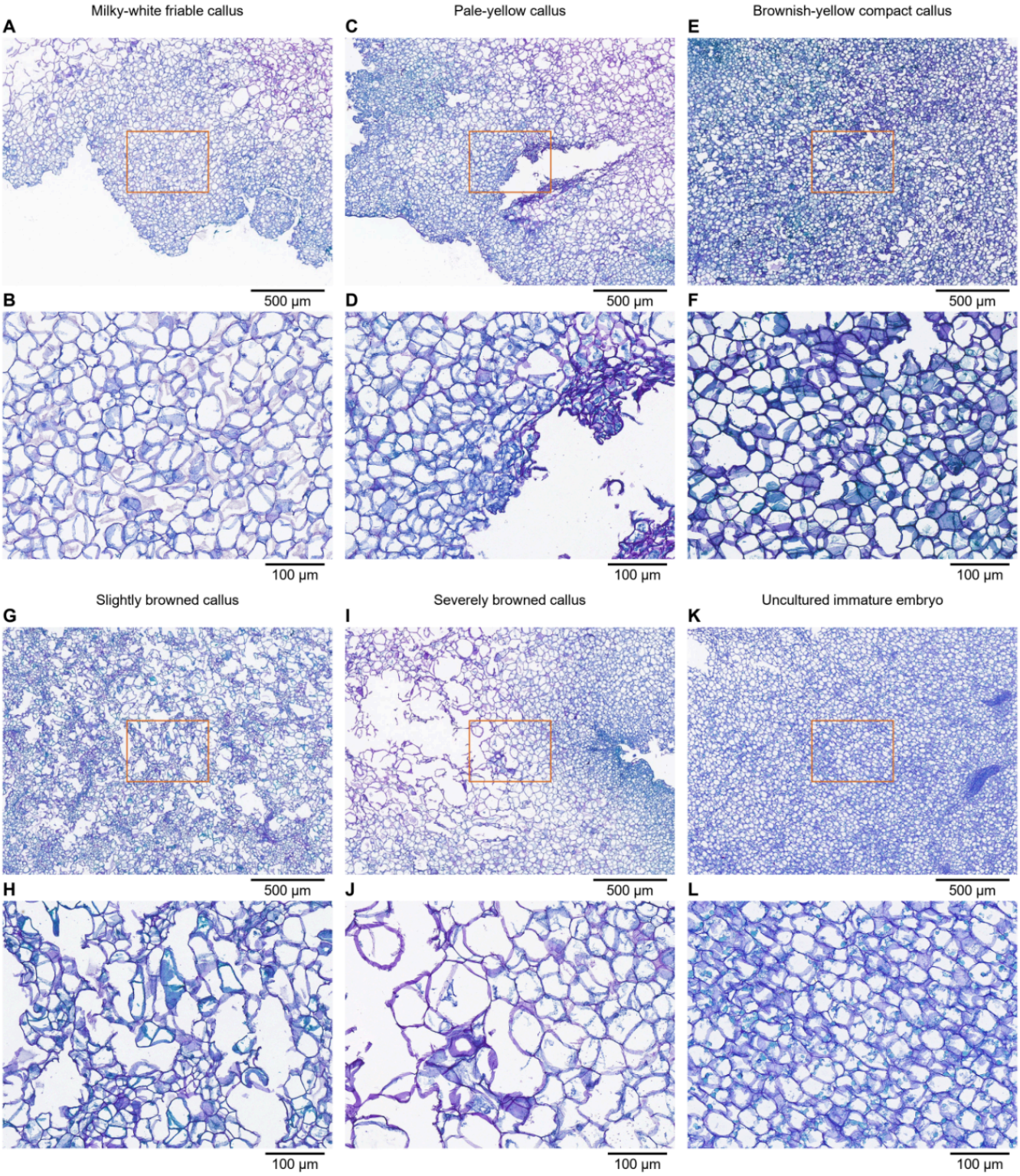


Figure 5

Histological organization of walnut tissues stained with toluidine blue. (A, B) Milky-white friable callus; (C, D) pale-yellow callus; (E, F) brownish-yellow compact callus; (G, H) slightly browned callus; (I, J) severely browned callus; and (K, L) uncultured immature embryo. Overview fields (A, C, E, G, I, K) and corresponding enlarged views (B, D, F, H, J, L) show cell arrangement and tissue continuity. Scale bars:

500 μm in overview fields and 100 μm in enlarged views. Fields are descriptive and are not independent biological replicates. Histological categories are not assigned to S1–S6

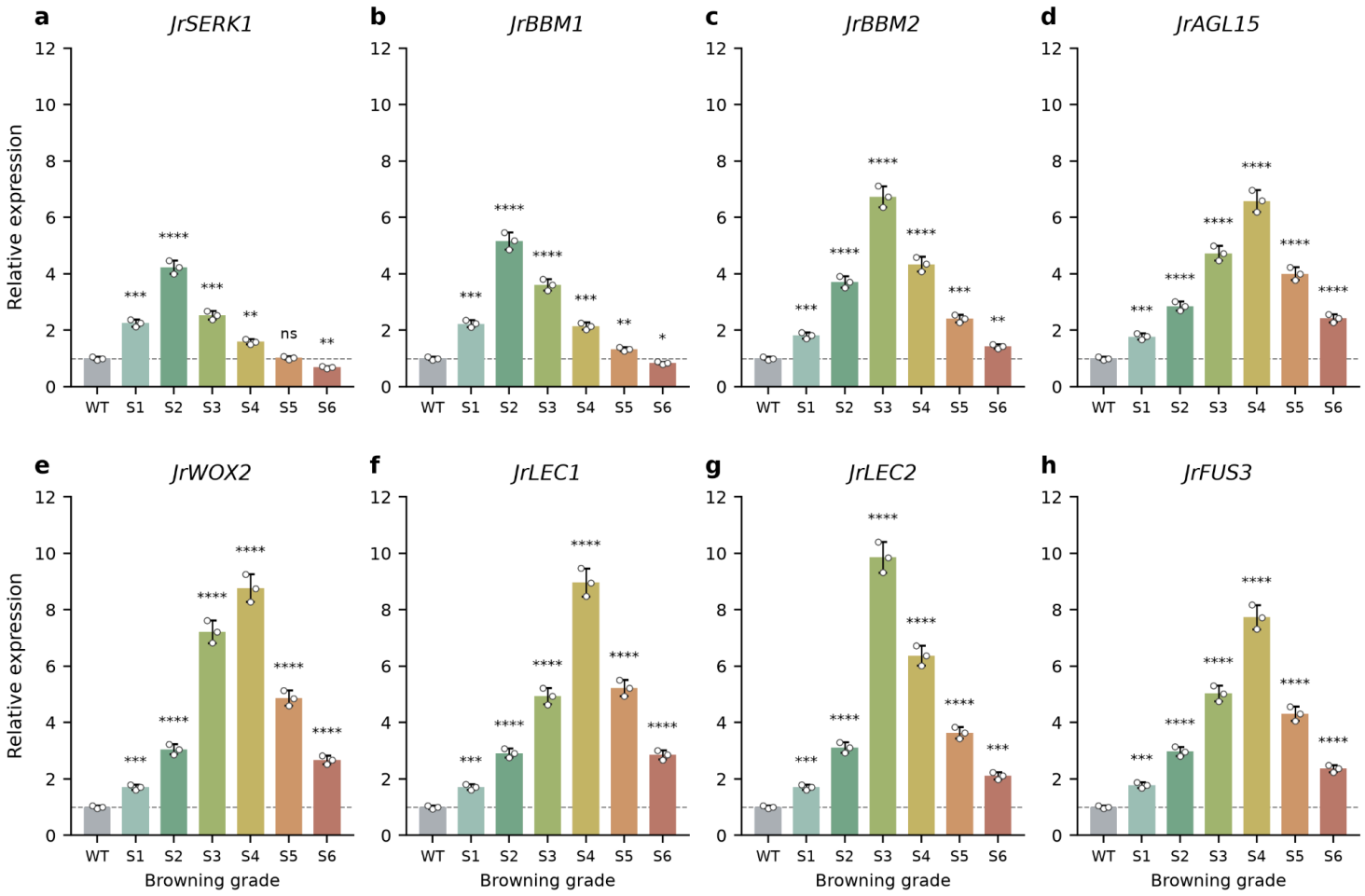


Figure 6

Expression of eight candidate embryogenesis-related genes in walnut tissues. (a) *JrSERK1*; (b) *JrBBM1*; (c) *JrBBM2*; (d) *JrAGL15*; (e) *JrWOX2*; (f) *JrLEC1*; (g) *JrLEC2*; and (h) *JrFUS3*. Bars and error bars show mean ± SD, and open circles show independent biological replicates (n = 3 per group). Relative expression was calculated using the $2^{-\Delta\Delta Ct}$ method with mean WT ΔCt as the calibrator and *JrTIP41* as the reference gene. Dashed lines indicate a relative expression of one. Significance symbols refer to two-sided Welch tests on ΔCt against WT, with Holm adjustment across six comparisons within each gene: ns, adjusted P ≥ 0.05; * P < 0.05; ** P < 0.01; *** P < 0.001; **** P < 0.0001. WT denotes uncultured cotyledons; S1–S6 denote browning grades. Replicate values and adjusted P values are provided in Online Resource 1, Tables S7 and S8

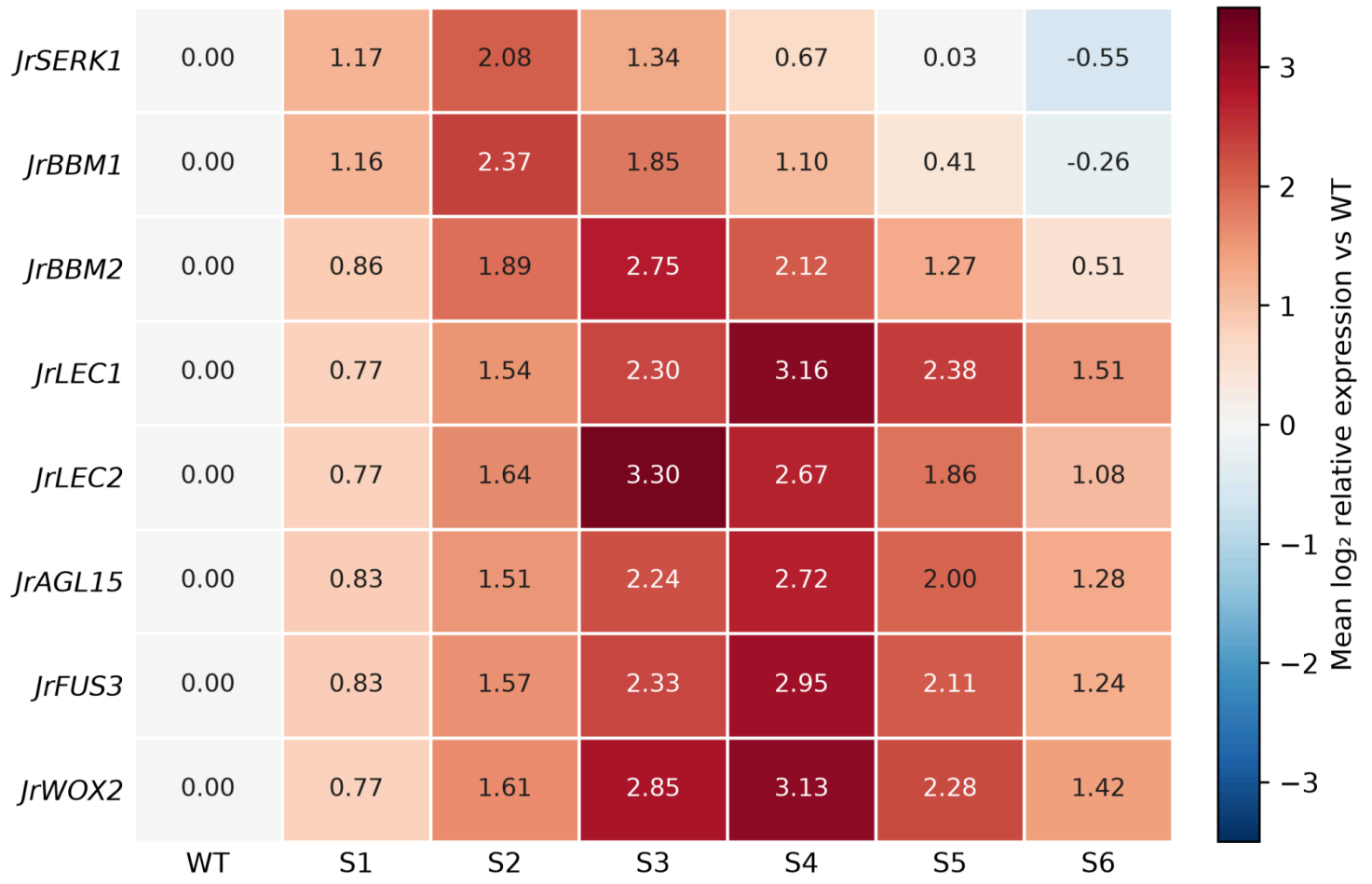


Figure 7

Heatmap of eight candidate embryogenesis-related genes in walnut callus browning grades S1–S6 and uncultured cotyledons (WT). Cell values represent mean $\log_2$ relative expression, calculated as mean WT ΔCt minus mean group ΔCt (−ΔΔCt; n = 3 biological replicates per group). *JrTIP41*was the sole reference gene. Red and blue indicate expression above and below WT, respectively, on a common scale centered on zero. Values were not row-standardized, and groups were not clustered. The heatmap summarizes expression patterns without displaying significance tests; biological-replicate variation and grade–WT comparisons are shown in Fig. 6 and Online Resource 1, Tables S7 and S8. S1–S6 denote browning grades rather than a time course

Supplementary Files

This is a list of supplementary files associated with this preprint. Click to download.

- REP1.pdf